

# PERFORMANCE OF SST $k-\omega$ TURBULENCE MODEL FOR COMPUTATION OF VISCOUS DRAG OF AXISYMMETRIC UNDERWATER BODIES

**M. M. Karim\***

*Dept. of Naval Architecture and Marine Engineering, Bangladesh University of Engineering and Technology (BUET),  
Dhaka-1000, Bangladesh  
[mmkarim@name.buet.ac.bd](mailto:mmkarim@name.buet.ac.bd)*

**M. M. Rahman**

*Doctoral Student, Department of Naval Architecture and Ocean Engineering, Graduate School of Engineering,  
Osaka University, Japan*

**M. A. Alim**

*Department of Mathematics, Bangladesh University of Engineering and Technology (BUET)  
Dhaka-1000, Bangladesh  
[maalim@math.buet.ac.bd](mailto:maalim@math.buet.ac.bd)*

\*Corresponding Author

(Received: November 20, 2009 – Accepted in Revised Form: May 25, 2010)

**Abstract** This paper presents 2-D finite volume method for computation of viscous drag based on Reynolds-averaged Navier-Stokes (RANS) equations. Computations are performed on bare submarine hull DREA and six axisymmetric bodies of revolution with a number of length-diameter ( $L/D$ ) ratios ranging from 4 to 10. Both structured and unstructured grids are used to discretize the domain around the bodies. Different turbulence models have been tested to simulate turbulent flow. The comparison of predicted results from 2-D method with published experimental/numerical results showed satisfactory conformity.

**Keywords** Axisymmetric Body of Revolution, Underwater Vehicle, Viscous Drag, CFD, Turbulence Model

چکیده این مقاله برای محاسبه گرانروی درگ به روش حجم محدود بر اساس معادلات رینولدز-متوسط ناوییه استوکس (RANS) بصورت دو بعدی را نشان میدهد. محاسبات بر روی زیردریایی برهنه (DREA) و جسم شش بعدی حاصل از دوران با نسبت طول به قطر ( $L/D$ ) 4 تا 10 صورت گرفته است. دامنه اطراف اجسام با هر دو شبکه شکل یافته و یا شکل نیافته منقطع شده است. برای آزمون صحت مدل سازی جریان آشفته از مدل های مختلف آشفته استفاده گردید. مقایسه نتایج پیش بینی شده از روش 2 بعدی با نتایج آزمایشی/عددی همخوانی مطلوبی داشته است.

## 1. INTRODUCTION

Computational Fluid Dynamics (CFD) has progressed rapidly in the past fifty years. It has been used in many industrial fields and plays an irreplaceable role in engineering design and

scientific research. However, due to complex geometry of ship, CFD has fallen behind its counterparts in other industrial fields. But with the recent breakthrough in CFD technology, practical applications of CFD in analyzing and predicting ship performance now become possible. Despite

the advance of Experimental Fluid Dynamics (EFD), the demand to know the detailed flow field with better resolution and near-wall flow information associated with the motion of a ship is beyond what the current experimental technology can offer. As the cost and time required for the computation are much lower than that of model tests, CFD has been involved in applied ship research and ship design. It has been used already in practical ship design for predicting the viscous flow around the hull, flow separations, viscous resistance, wake field, appendage alignment, propeller/hull interaction etc.

Viscous flow computation for ship hull began in 1960s with the simplified boundary layer equation being solved. In this early approach, the boundary layer over most of the hull can be satisfactorily calculated within required engineering accuracy. However, this approach failed in predicting flow at stern and into the wake. This prompted the researchers to go for more advanced method. During the 1980s large number of RANS (Reynolds Averaged Navier-Stokes) solvers was developed for ship stern flow. Later, the stern flow prediction was improved rather remarkably around 1990. However, CFD simulations near the propeller were less satisfactory due to inaccurate prediction of the bilge vortex and resultant characteristic “hook” shape in the boundary layer. Later it was realized that the reason for the inability to predict the wake hook was the inadequate modeling of turbulence. So quite a lot of effort was spent on finding an appropriate turbulence model for ship stern flow in the next few years and this had led to the adoption of more advanced models, such as the  $k-\varepsilon$  turbulence model and the  $k-\omega$  turbulence model.

However, effective utilization of CFD for marine hydrodynamics depends on proper selection of turbulence model, grid generation and boundary resolution. Simulation of underwater hydrodynamics continues to be based on the solution of the Reynolds-averaged Navier-Stokes (RANS) equations. Although minimization of drag is one of the most important design criteria, not much effort has been given to determining viscous drag, an important parameter in the development of a new design. This paper presents finite volume method for computation of viscous drag based on Reynolds-averaged Navier-Stokes (RANS)

equations. Various researchers used turbulence modeling to simulate flow around axisymmetric bodies since late seventies. Patel and Chen [1] made an extensive review of the simulation of flow past axisymmetric bodies. Choi and Chen [2] gave calculation method for the solution of RANS equation, together with  $k-\varepsilon$  turbulence model. Sarkar et al [3] used a low-Re  $k-\varepsilon$  model of Lam and Bremhorst [4] for simulation of flow past underwater axisymmetric bodies. In this research, SST  $k-\omega$  model is used to simulate complete turbulent flow past underwater vehicle hull forms. The body used for this purpose is a standard DREA (Defence Research Establishment Atlantic) bare submarine hull [5] as shown in Fig. 1 and six axisymmetric bodies of revolution based on Gertler’s geometry [6].

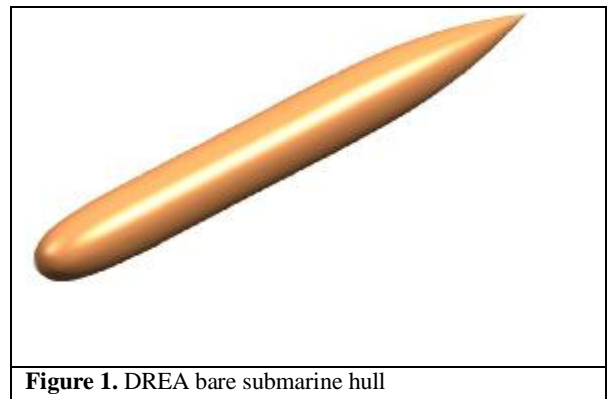


Figure 1. DREA bare submarine hull

## 2. THEORETICAL FORMULATION

Using the standard  $k-\omega$  model of turbulence the continuity and general form of transport equations for the incompressible flow past an axisymmetric body, i.e., a typical autonomous underwater vehicle (AUV) hull form take the following form in cylindrical coordinates:

$$\frac{\partial}{\partial x}(rru) + \frac{\partial}{\partial r}(rrv) = 0 \quad (1)$$

$$\frac{\partial}{\partial t}(rrf) + \frac{\partial}{\partial x}(rruf) + \frac{\partial}{\partial r}(rrvf) = \quad (2)$$

$$\frac{\partial}{\partial x}\left(r\Gamma_f \frac{\partial f}{\partial x}\right) + \frac{\partial}{\partial r}\left(r\Gamma_f \frac{\partial f}{\partial r}\right) + rS_f$$

where  $f$  represents general dependent variables  $u$ ,

$v$ ,  $k$  and  $\omega$ .  $u$  and  $v$  are the velocity components in the  $x$  and  $r$  directions respectively,  $k$  is the turbulent kinetic energy,  $\omega$  is the rate of dissipation of kinetic energy,  $\rho$  is the density of the fluid,  $G_f$  is the effective diffusion coefficient and  $S_f$  denotes the source of  $f$ .

**2.1 The Shear-Stress Transport (SST)  $k$ - $\omega$  Model** The SST  $k$ - $\omega$  turbulence model is a two-equation eddy-viscosity model developed by Menter [7] to effectively blend the robust and accurate formulation of the  $k$ - $\omega$  model in the near-wall region with the free-stream independence of the  $k$ - $\varepsilon$  model in the far field. To achieve this, the  $k$ - $\varepsilon$  model is converted into a  $k$ - $\omega$  formulation. The SST  $k$ - $\omega$  model is similar to the standard  $k$ - $\omega$  model, but includes the following refinements:

- The standard  $k$ - $\omega$  model and the transformed  $k$ - $\varepsilon$  model are both multiplied by a blending function and both models are added together.
- The blending function is designed to be one in the near-wall region, which activates the standard  $k$ - $\omega$  model, and zero away from the surface, which activates the transformed  $k$ - $\varepsilon$  model.
- The SST model incorporates a damped cross-diffusion derivative term in the  $\omega$ -equation.
- The definition of the turbulent viscosity is modified to account for the transport of the turbulent shear stress.
- The modeling constants are different.

These features make the SST  $k$ - $\omega$  model more accurate and reliable for a wider class of flows (e.g., adverse pressure gradient flows, airfoils, transonic shock waves) than the standard  $k$ - $\omega$  model.

The shear-stress transport (SST)  $k$ - $\omega$  model is so named because the definition of the turbulent viscosity is modified to account for the transport of the principal turbulent shear stress. The use of a  $k$ - $\omega$  formulation in the inner parts of the boundary layer [8] makes the model directly usable all the way down to the wall through the viscous sub-layer; hence the SST  $k$ - $\omega$  model can be used as a Low-Re turbulence model without any extra damping functions. The SST formulation also

switches to a  $k$ - $\varepsilon$  behaviour in the free-stream and thereby avoids the common  $k$ - $\omega$  problem that the model is too sensitive to the inlet free-stream turbulence properties. It is this feature that gives the SST  $k$ - $\omega$  model an advantage in terms of performance over both the standard  $k$ - $\omega$  model and the standard  $k$ - $\varepsilon$  model. Other modifications include the addition of a cross-diffusion term in the  $\omega$  equation and a blending function to ensure that the model equations behave appropriately in both the near-wall and far-field zones.

Transport equations for the SST  $k$ - $\omega$  model are given by:

$$\frac{\partial}{\partial t}(rk) + \frac{\partial}{\partial x_i}(rku_i) = \frac{\partial}{\partial x_j} \left( \Gamma_k \frac{\partial k}{\partial x_j} \right) \quad (3)$$

$$\begin{aligned} & + \tilde{G}_k - Y_k + S_k \\ & \frac{\partial}{\partial t}(r\omega) + \frac{\partial}{\partial x_i}(r\omega u_i) = \\ & \frac{\partial}{\partial x_j} \left( \Gamma_\omega \frac{\partial \omega}{\partial x_j} \right) + G_\omega - Y_\omega + D_\omega + S_\omega \end{aligned} \quad (4)$$

In these equations,  $\tilde{G}_k$  represents the generation of turbulence kinetic energy due to mean velocity gradients,  $G_\omega$  represents the generation of  $\omega$ ,  $\Gamma_k$  and  $\Gamma_\omega$  represent the effective diffusivity of  $k$  and  $\omega$ , respectively,  $Y_k$  and  $Y_\omega$  represent the dissipation of  $k$  and  $\omega$  due to turbulence,  $D_\omega$  represents the cross-diffusion term,  $S_k$  and  $S_\omega$  are source terms.

**2.2 Boundary Conditions** Since the geometry of an axisymmetric underwater hull is, in effect, a half body section rotated about an axis parallel to the direction of the free stream velocity, the bottom boundary of the domain is modeled as an axis boundary. Additionally, the left and top boundaries of the domain are modeled as velocity inlet, the right boundary is modeled as an outflow boundary, and the surface of the body itself is modeled as a wall. The inlet condition for turbulence kinetic energy  $k$  and specific dissipation rate  $\omega$  are calculated from

$$k = \frac{3}{2} (U_{avg} l)^2 \quad \text{and} \quad \omega = \frac{k^{\frac{1}{2}}}{C_m \frac{1}{4} l}, \quad \text{respectively.}$$

Where,  $U_{avg}$  is the mean flow velocity, turbulence intensity  $I=0.16(Re)^{-1/8}$  turbulence length  $l=0.07L$ . The constants in SST  $k$ - $\omega$  model are considered as:

$\sigma_{k,1} = 1.176$ ,  $\sigma_{\omega,1} = 2.0$ ,  $\sigma_{k,2} = 1.0$ ,  $\sigma_{\omega,2} = 1.168$ ,  $\alpha_f = 0.31$ ,  $\beta_{i,1} = 0.075$ ,  $\beta_{i,2} = 0.0828$ ,  $\kappa = 0.41$ ,  $C_\mu = 0.09$ .

**2.3 Viscous Drag** The viscous drag of a body is generally derivable from the boundary-layer flow either on the basis of the local forces acting on the surface of the body or on the basis of the velocity profile of the wake far downstream. The local hydrodynamic force on a unit of surface area is resolvable into a surface shearing stress or local skin friction tangent to the body surface and a pressure  $p$  normal to the surface. The summation over the whole body surface of the axial components of the local skin friction and of the pressure gives, respectively, the skin-friction drag  $D_f$  and the pressure drag  $D_p$  which for a body of revolution in axisymmetric flow become

$$D_f = 2p \int_0^{x_e} r_w t_w \cos a \, dx \quad (5)$$

$$D_p = 2p \int_0^{x_e} r_w p \sin a \, dx \quad (6)$$

where  $r_w$  is the radius from the axis to the body surface,  $a$  is the arc length along the meridian profile, and  $x_e$  is the total arc length of the body from nose to tail.

The sum of the two drags then constitutes the total viscous drag,  $D$  or  $D = D_f + D_p$

The drag coefficient,  $C_D$  and the pressure coefficient,  $C_p$  based on some appropriate reference area  $A$  are given by:

$$\left. \begin{aligned} C_D &= \frac{D}{0.5 r U_\infty^2 A} \\ C_p &= \frac{p - p_\infty}{0.5 r U_\infty^2 A} \end{aligned} \right\} \quad (7)$$

Where  $p_\infty$  is pressure of free stream and  $U_\infty$  is free stream velocity.

### 3. METHODOLOGY

**3.1 Numerical Method** Two-dimensional axisymmetric RANS equations are the governing equations in this study and they are solved numerically. The numerical solution is

worked out through adopting a cell-centered finite volume method [9, 10]. The governing equations are discretized using a second order upwind interpolation scheme and the discretized equations are solved using PISO algorithm [9]. The solution is considered converged when the normalized residuals of all the variables fall below  $10^{-5}$ .

**3.2 Geometry of Axisymmetric Underwater Vehicle (AUV) Hull Form** Axisymmetric bodies are ideal candidates for a parametric study with their easily defined geometry, straightforward grid generation, and available experimental data. At first the bare submarine hull DREA and then a systematic series of mathematically defined bodies of revolution is studied.

#### 3.2.1 Geometry of bare submarine hull DREA

The parent axisymmetric hull form [5] with maximum length,  $l$  and diameter,  $d$  can be divided into three regions, i.e., nose, mid body and tail.

(i) The nose can be represented by:

$$\frac{r_1(x)}{l} = \frac{d}{l} \left[ 2.56905 \sqrt{\frac{x}{l}} - 3.48055 \frac{x}{l} + 0.49848 \left( \frac{x}{l} \right)^2 + 3.40732 \left( \frac{x}{l} \right)^3 \right] \quad (8)$$

$; 0 \leq \frac{x}{l} \leq 0.2$

(ii) The mid body (circular cylinder) is given by:

$$\frac{r_2(x)}{l} = \frac{d}{2l}; 0.2 \leq \frac{x}{l} \leq 1 - \frac{3d}{l} \quad (9)$$

(iii) The tail is represented by:

$$\frac{r_3(x)}{l} = \frac{d}{2l} - \frac{l}{18d} \left[ \frac{x}{l} - \left( 1 - \frac{3d}{l} \right) \right]^2; 1 - \frac{3d}{l} \leq \frac{x}{l} \leq 1 \quad (10)$$

#### 3.2.2 Geometry of axisymmetric body of revolution

Each body is defined by a sixth-degree polynomial [6]. Six axisymmetric bodies are generated with length-to-diameter ratios ( $L/D$ ) ranging from four to ten. All bodies are evaluated at zero angle of attack.

#### 3.3 Computational Domain and Grid Generation

The computational domain extended  $1.0L$  upstream of the leading edge of the axisymmetric body,  $1.0L$  above the body surface and  $2.0L$  downstream from the trailing edge; where  $L$  is the overall length of the

body. The solution domain is found large enough to capture the entire viscous-inviscid interaction and the wake development.

Both structured and unstructured grids are constructed on DREA and AUV hulls. At first a body-fitted H-type structured grid with quadrilateral cell is used to mesh the computational domain shown in Fig. 2.

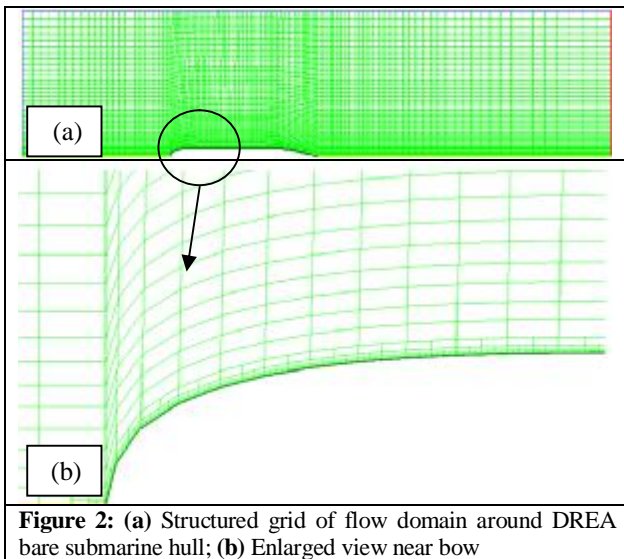


**Figure 2:** (a) Structured grid of flow domain around DREA bare submarine hull; (b) Enlarged view near bow

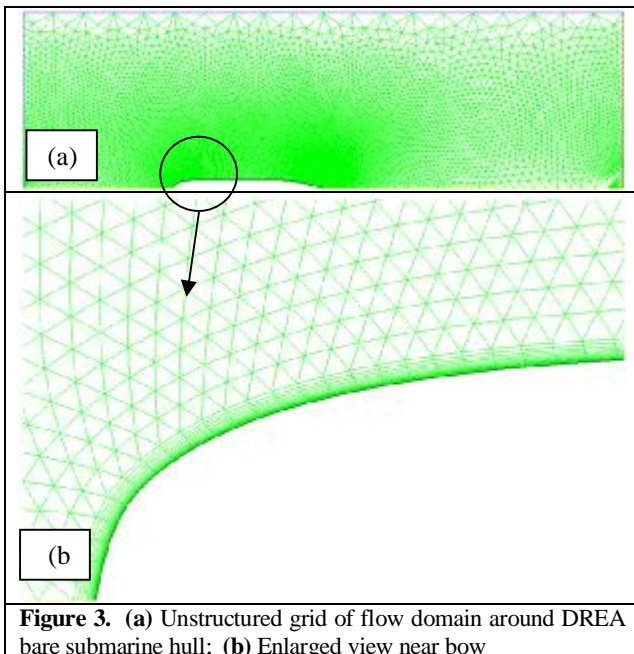


**Figure 3:** (a) Unstructured grid of flow domain around DREA bare submarine hull; (b) Enlarged view near bow

Then the unstructured pave mesh with triangular cell is formed around the axisymmetric bodies. In

both of the cases more cells are concentrated near the hull surface to capture the viscous drag. In addition, a boundary layer is created around the body surface in case of the unstructured grid shown in Fig.3.

In external flow simulations using SST  $k-\omega$  the computational grid should be in such a way that sufficient number of grid points remain within the laminar sub-layer of the ensuing boundary layer. In order to ensure this, usually the  $y^+$  criterion is used.  $y^+$  is a non-dimensional distance from the body wall and is defined as  $y^+ = yu_t / \nu$ , where  $u_t = \tau_w / \rho$  is friction velocity and  $\nu$  kinematic viscosity. The  $y^+$  criterion states that first grid point normal to the body wall should not lie beyond  $y^+ = 4.0$  and for reasonable accuracy at least five points should lie within  $y^+ = 11.5$  [4]. This criterion is followed in this study as the average value of  $y^+$  doesn't exceed the prescribed limit as shown in Fig. 4.

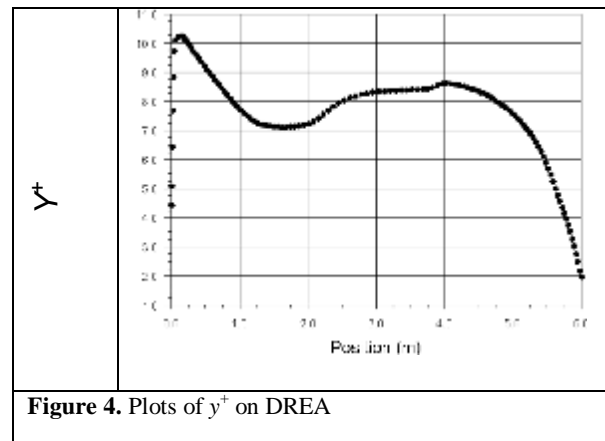


**Figure 4.** Plots of  $y^+$  on DREA

#### 4. RESULTS AND DISCUSSIONS

The intent of this study is to investigate the flow visualization and to calculate the viscous drag around the axisymmetric underwater vehicle hull in case of fully turbulent flow. Much effort has been given for selecting appropriate grid using structured and unstructured grid on both of the bodies. As the geometrical shape of the two bodies are almost identical, similar grid independence check has been done on them. Table 1 shows the drag coefficient computed on DREA hull for different structured grid. From this table it is observed that the structured grid containing 14859

quadrilateral cells give better result and not much improvement is occurred with the increment of cell number. However, with unstructured grid it is found that 27,000 mixed cells give best result.

To select a suitable turbulence model for this type of simulation different turbulence models are tested. Table 2 shows the drag coefficient computed by authors on AUV with  $L/D = 4$  using different turbulence models at Reynolds number  $2.0 \times 10^7$ . From this table it may be concluded that the SST  $k-\omega$  turbulence model computes more accurate drag coefficient for slender bodies. Fully turbulent flow is simulated in both of the cases but different Reynolds numbers are chosen depending on the availability of experimental and/or numerical data.

**TABLE 1: The Drag Coefficient Computed on DREA Hull for Different Structured Grid at  $Re = 2.3 \times 10^7$**

| No. of Cell (Quadrilateral) | $C_D (\times 10^{-3})$ | Experimental $C_D$                 |
|-----------------------------|------------------------|------------------------------------|
| 5016                        | 1.3899                 | $1.23 \times 10^{-3} \pm 0.000314$ |
| 9603                        | 1.2838                 |                                    |
| 12639                       | 1.0377                 |                                    |
| 13164                       | 1.0358                 |                                    |
| 13809                       | 1.0348                 |                                    |
| 14859                       | 1.0325                 |                                    |

**TABLE 2: The Drag Coefficient Computed on AUV with  $L/D = 4$  using Different Turbulence Models at Reynolds Number  $2.0 \times 10^7$**

| Turbulence model            | Drag coefficient, $C_D (\times 10^{-3})$ | Experimental $C_D (\times 10^{-3})$ [6] |
|-----------------------------|--|---|
| Sparat Allmaras (S-A)       | 5.50                                     | 3.208                                   |
| $k-\varepsilon$ (standard)  | 6.0                                      |   |
| $k-\varepsilon$ (relizable) | 4.23                                     |   |
| $k-\omega$ (standard)       | 6.01                                     |   |
| (SST) $k-\omega$            | 3.435                                    |   |

The computation of drag coefficient for bare

submarine hull DREA is performed using SST  $k-\omega$  turbulence model at Reynolds number of  $2.3 \times 10^7$  and shown in Table 3. From the table it is seen that the computed values both for structured and unstructured grid agree well with the experimental results published by Department of Research and Development Canada- Atlanta, National Defense [11]. It is also noted that present results using structured and unstructured grids are more accurate than that computed by Baker [5]. Fig. 5 indicates the convergence history of the drag coefficient on DREA hull.

**TABLE 3: Comparison of Computed Drag Coefficients with Experimental Values for Submarine DREA Hull.**

|                     | $C_D$ (Structured) | $C_D$ (Unstructured) | $C_D$ (Exp. [11])      | $C_D$ (Baker [5]) |
|---------------------|--------------------|----------------------|------------------------|-------------------|
| Submarine hull DREA | 0.0010325          | 0.00135              | $0.00123 \pm 0.000314$ | 0.00167           |

It is known that the total drag coefficient ( $C_D$ ) is composed of pressure coefficient ( $C_p$ ) and frictional coefficient ( $C_f$ ), which are obtained by integrating the pressure distribution and viscous shear stress, respectively, over the body surface.

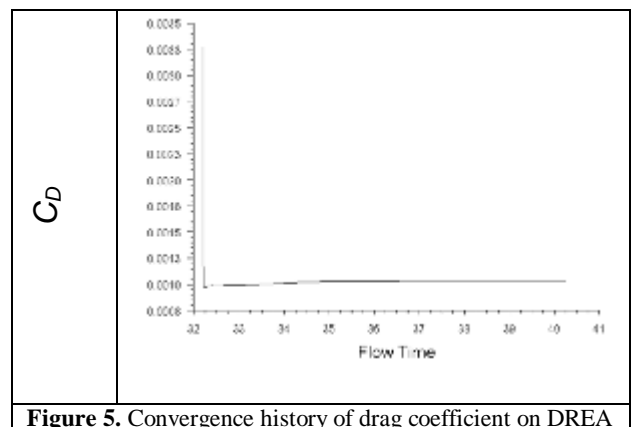


**Figure 5.** Convergence history of drag coefficient on DREA

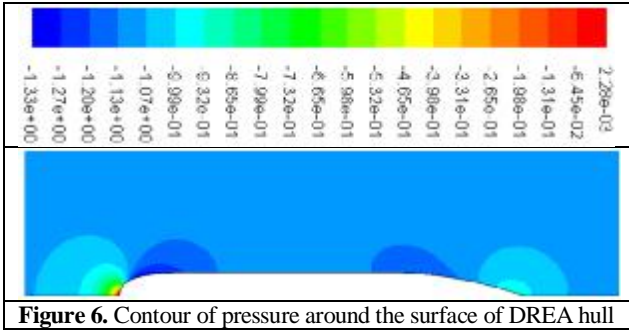


Figure 6. Contour of pressure around the surface of DREA hull

The contours of pressure and velocity distribution on DREA are also shown in Fig. 6 and Fig. 7 respectively. Both figures give the expected distribution of pressure and velocity using different color and scale.

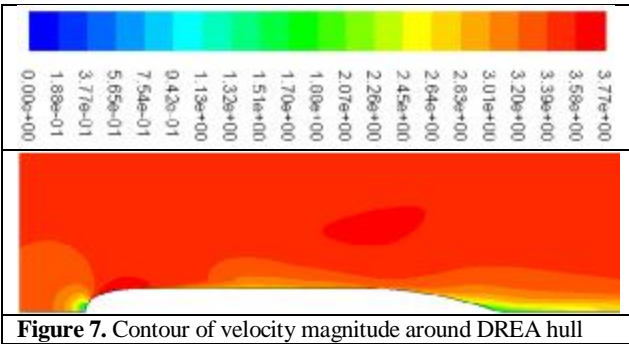


Figure 7. Contour of velocity magnitude around DREA hull

Then the study has been extended to calculate the drag coefficient around six axisymmetric bodies ranging from  $L/D$  ratio from 4 to 10 at  $Re = 2.0 \times 10^7$  using SST  $k-\omega$  turbulence model. Several prediction methods have been investigated to calculate the drag for this series of bodies.

TABLE 4: Drag Coefficient ( $C_D \times 10^{-3}$ ) from Different Prediction Methods at  $Re = 2 \times 10^7$  for  $L/D = 4-10$

| $L/D$ | White's formula (1977) | B.L theory | Lin <i>et al.</i> (1995) (ISFLOW) | Present      |                | Experimental [6] |
|-------|------------------------|------------|-----------------------------------|--------------|----------------|------------------|
|       |                        |            |                                   | (Structured) | (unstructured) |                  |
| 4     | 3.108                  | 3.028      | 3.213                             | 3.435        | 3.184          | 3.208            |
| 5     | 2.998                  | 2.958      | 2.948                             | 3.140        | 2.983          | 2.988            |
| 6     | 2.928                  | 2.898      | 2.858                             | 3.020        | 2.814          | 2.848            |
| 7     | 2.858                  | 2.858      | 2.761                             | 2.958        | 2.716          | 2.758            |
| 8     | 2.808                  | 2.818      | 2.691                             | 2.893        | 2.647          | 2.718            |
| 10    | 2.738                  | 2.778      | 2.629                             | 2.815        | 2.574          | 2.703            |

Table 4 provides a comparison of the current results with the experimental and other three methods; one,

based on a differential boundary layer formulation (theory of Cebeci and Smith), another based on a simple drag formula by White [12] and the other computed numerically using ISFLOW by Lin *et al* [13]. The computed results are satisfactory and discrepancies arise mainly due to assumption of 2-D axisymmetric flow without considering 3-D effect. However, results by this method are promising because of the cost effectiveness of the method. It is also noted that results computed with unstructured grid gives higher accuracy.

From Table 4 it is also observed that drag coefficient is decreasing with the increase of length-diameter ratio. In other words, the drag force is inversely proportional to  $L/D$  ratio of the body. It happened because the shape of the body is transforming from thick to slender with the increase of  $L/D$  as the body length is fixed. The fineness ratio  $L/D$  influences substantially the resistance of submarines, since the wetted surface depends strongly on it for a given volume. Therefore reduction in the wetted surface reduces the resistance. The plot of velocity vectors are shown in Fig. 8. From enlarged view of velocity vectors, change in velocity within the boundary layer and vortex near stern are clearly visible.

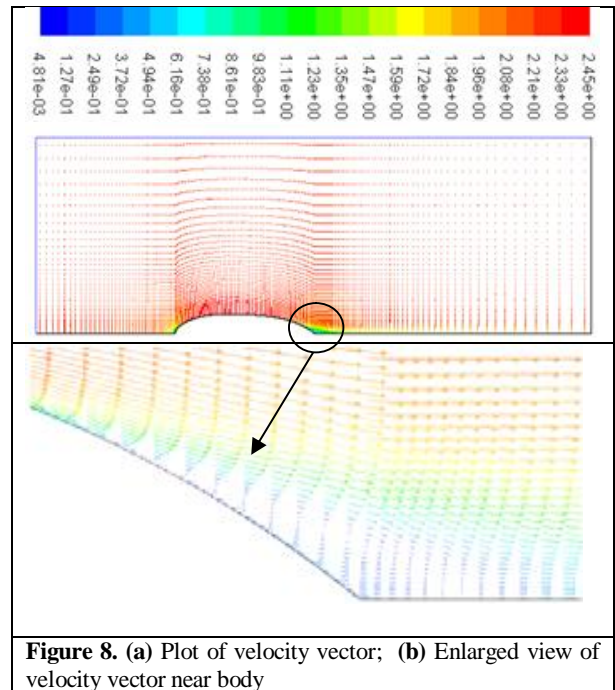


Figure 8. (a) Plot of velocity vector; (b) Enlarged view of velocity vector near body

## 5. CONCLUSION

Numerical computation of viscous drag for axisymmetric underwater vehicle is performed using 2-D finite volume method based on Reynolds-averaged Navier-Stokes equations. Among different models, Shear Stress Transport (SST)  $k-\omega$  model shows better performance. The results computed by the cost effective 2-D method seem very promising with respect to published results computed by 3-D method and also experimental measurements.

## 6. REFERENCES

1. Patel, V. C., Chen, H.C., "Flow over tail and in wake of axisymmetric bodies: review of the state of the art", *Journal of Ship Research*, Vol. 30, No. 3, (1986), pp. 202-314.
2. Choi, S. K., Chen, C. J., "Laminar and turbulent flows past two dimensional and axisymmetric bodies", *Iowa Institute of Hydraulic Research, IIHR Report 334-II* (1990).
3. Sarkar, T., Sayer P. G., Fraser, S. M., "A study of autonomous underwater vehicle hull forms using computational fluid dynamics", *International Journal for Numerical Methods in Fluids*, Vol. 25, (1997), pp. 1301-1313.
4. Lam, C.K.G., Bremhorst, K., "A modified form of the  $k-\epsilon$  model for predicting wall turbulence", *ASME Journal Fluid Engineering*, Vo.103, (1981), pp. 456.
5. Baker, C., "Estimating drag forces on submarine hulls", *Report DRDC Atlantic CR 2004-125*, Defence R&D Canada – Atlantic, (2004).
6. Gertler, M., "Resistance experiments on a systematic series of streamlined bodies of revolution for application to the design of high speed submarines", *DTMB Report C-297* (1950).
7. Menter, F. R., "Two-equation eddy-viscosity turbulence models for engineering applications". *AIAA Journal*, Vol. 32(8), (1994), pp.1598-1605.
8. Schlichting, H., "Boundary Layer Theory", *McGraw-Hill, New York*, (1966).
9. Versteeg, H. K., Malalasekera, W., "An Introduction to Computational Fluid Dynamics The Finite Volume Method", *Longman Scientific and Technical, U.K.* (1995).
10. Cebeci, T., Shao, J.R., Kafyeke, F., Laurendeau, E., "Computational Fluid Dynamics for Engineers", *Horizons Publishing Inc., Long Beach, California* (2005).
11. Department of Research and Development Canada-Atlanta, National Defense, "Wind Tunnel Test of the DREA Six Meter long Submarine Model- Force Data analysis", Ottawa, (1988).
12. White, N. M., "A comparison between a simple drag formula and experimental drag data for bodies of revolution", *DTNSRDC Report 77-0028* (1977).
13. Lin, C.W., Percival, S. and Gotimer, E.H., "Viscous Drag Calculations for Ship Hull Geometry", Technical Report, Design Evaluation Branch, Hydromechanics Directorate, *David Taylor Model Basin, Carderock Division Naval Surface Warfare Center, Bethesda, MD USA*, (1995)